Received: 6 June 2025 | Revised: 7 August 2025 | Accepted: 8 September 2025

DOI: 10.1111/jace.70276

Journal of the American Ceramic Society

SPECIAL ISSUE ARTICLE

Hollow skeletal macroporous aluminum hydroxide monoliths and their calcined derivatives with high diffuse reflectance

Gen Hayase

Research Center for Electronic and Optical Materials, National Institute for Materials Science, Tsukuba, Japan

Correspondence
Gen Hayase, Research Center for Electronic and Optical Materials, National Institute for Materials Science, 1-1 Namiki, Tsukuba 305-0044, Japan.
Email: gen@aerogel.jp

A previous version of this manuscript has been deposited on a preprint server (https://doi.org/10.26434/chemrxiv-2025-3nz7d-v2)

Abstract

Macroporous aluminum hydroxide monoliths with continuous hollow skeletons were fabricated through a scalable, template-free sol–gel synthesis from metal–salt precursors. Tuning the concentration of propylene oxide, which serves as a proton scavenger, yielded crack-free monoliths several centimeters in diameter. Scanning electron microscopy revealed a three-dimensional porous network composed of an interconnected nanoplatelet shell. The as-prepared sample exhibited a Brunauer–Emmett–Teller-specific surface area of 429 $m^2\ g^{-1}$. Calcination at 500°C converted the framework into γ-alumina while preserving the hollow architecture and a high specific surface area of 314 $m^2\ g^{-1}$. Subsequent heating to 1250°C produced α-alumina while preserving the monolithic shape and continuity of the skeletal framework; however, the hollow structure collapsed, and the surface area decreased significantly. Optical measurements showed that aluminum hydroxide and α-alumina monoliths both exhibited high total diffuse reflectance across the ultraviolet–visible–near-infrared (UV–Vis–NIR) range (400–1200 nm), comparable to Spectralon. The α-alumina retained over 90% reflectance up to 2500 nm and demonstrated excellent thermal stability. These results suggest that the fabricated monoliths could be used as diffuse reflectance reference materials.

KEYWORDS
alumina, optical materials/properties, porous materials, sol–gel

1 | INTRODUCTION

Macroporous monoliths possess continuous three-dimensional skeletal networks and hierarchically ordered pores. They have been widely applied in fields such as catalyst supports, adsorbents, sensors, and separation membranes.[1] Compared to particulate porous materials, these monoliths exhibit superior mechanical strength and fluid transport properties, making them particularly attractive as media for chemical reactions and separations. In addition to the continuous macropores at the microscopic level, incorporating mesopores and micropores within the skeleton can further optimize reactivity and mass-transport characteristics. Sol–gel

methods are among the most widely employed fabrication strategies for producing such macroporous monoliths. In ceramic processing, the sol–gel method involves the hydrolysis and condensation of metal alkoxides or metal oxide precursors to form a gel. This gel is then dried and calcined to produce a porous solid. Sol–gel processes involving phase separation allow for control over macropore formation during gelation, making them suitable for producing centimeter-scale monoliths.[2,3] The resulting uniform porous structures have been explored for practical applications as separation media and catalysts.

Numerous reports exist on hierarchical monoliths with mesopores or micropores embedded within the skeleton. However, reports on monoliths whose skeletal frameworks are intrinsically hollow are scarce. In contrast, hollow ceramic materials in particulate form have been extensively studied. Common fabrication methods include hard-template and soft-template approaches.[4] These methods have also been successfully applied to aluminum hydroxide [$Al(OH)_3$] and aluminum oxide (Al_2O_3) systems.[5] In the hard-template approach, a precursor is coated onto surfaces of templates, such as polystyrene beads. The template is then removed by calcination to obtain the hollow structure.[6] The soft-template approach uses surfactants or micelles in microemulsions to produce hollow nanoparticles.[5,7–9] In boehmite (AlOOH)-based systems, hydrothermal treatment allows for the formation of hollow particles through dissolution and reprecipitation.[10–12] These hollow particles have been investigated for potential applications in adsorption, drug delivery, catalysis, and optical materials.[10,13–16]

One of the few reported approaches for forming hollow structures within porous monoliths is atomic layer deposition (ALD).[17,18] In this method, ultrathin films are deposited onto a template surface. Subsequent template removal yields hollow architecture. However, the slow deposition rate, high equipment cost, and limited scalability of ALD restrict its practical applicability, especially for large-area or high-volume production. Additionally, increasing the thickness of the resulting structures poses a significant challenge from the perspective of gas diffusion.

In this study, I developed a scalable route for centimeter-scale macroporous monoliths possessing hollow skeletons by exploiting phase separation during a metal–salt-derived sol–gel process. With this approach, the hollow structure formed along the phase-separated interfaces. Sequential calcination of the aluminum hydroxide monolith yielded γ-alumina and, subsequently, α-alumina. Since no hard templates are needed, the process is simplified and scalable. Moreover, using metal salts offers practical advantages, such as reducing the cost of raw materials, enabling milder reaction conditions, and facilitating solution preparation. Previously, Tokudome et al. reported on the fabrication and structural control of macroporous alumina monoliths using metal salts. However, their method was limited to 10 mm-scale samples and did not yield hollow structures.[19,20] In the present work, I overcame this limitation by establishing a reproducible procedure that yields crack-free monoliths up to 50 mm in diameter.

The optical properties of the resulting hollow porous monoliths and their potential applications were also investigated. The hollow structure enhances light scattering, which is expected to provide high light diffusion performance.[21–23] Additionally, upon calcination, α-alumina loses hydroxyl groups and is expected to exhibit higher reflectance in the near-infrared (NIR) region than conventional materials, such as barium sulfate. This paper discusses the development of these hollow monolithic structures and their potential use as light-diffusive reflective materials.

2 | EXPERIMENTAL AND METHODS

2.1 | Materials

Aluminum chloride hexahydrate ($AlCl_3{\cdot}6H_2O$, >97.0%), propylene oxide (PO, >98.0%), and ethanol (>99.5%) were obtained from Kanto Chemical Co., Inc. Polyethylene oxide (PEO; Mw ~1 000 000, containing 200–500 ppm butylated hydroxytoluene as inhibitor) was purchased from Merck. All reagents were used as received.

2.2 | Sample preparation

Aluminum hydroxide porous monoliths were reproducibly prepared by a sol–gel process as follows. A stock solution of water and ethanol (volume ratio 4:6) was pre-mixed and used as the solvent throughout the experiments. In a typical preparation, 10 mL of the water–ethanol mixture and 5.0 g of $AlCl_3{\cdot}6H_2O$ were combined in a glass tube, to which 0–0.08 g of PEO was optionally added depending on the composition. Subsequently, PO in the range of 4.0–8.0 mL was added dropwise while maintaining the reaction mixture in a water bath at room temperature (~22°C). The mixture was stirred for 1 min before being transferred into a sealed mold. The sol was then heated at 40°C for 24 h to induce gelation and aging. The gelation times for representative PO amounts were approximately 20 min for 4.0 mL, 3 min for 6.0 mL, and 2 min for 8.0 mL. After aging, the resulting gel was demolded, washed by immersion in ethanol, and subjected to evaporative drying

to obtain monolithic xerogels. The samples were denoted as AM*x*-*y*, where *x* and *y* represent the amounts (in mL and g, respectively) of PO and PEO used in the initial formulation. Various compositions with different amounts of PO and PEO were explored in preliminary trials to determine suitable conditions for fabricating crack-free monoliths. Only selected formulations were characterized in detail. Some of the aluminum hydroxide monoliths were calcined in air using an electric furnace (ROP-001H, AS ONE Corp.) at 500°C for 2 h or at 1250°C for 2 h.

2.3 | Characterization

The microstructure of the samples was examined using a scanning electron microscope (SEM) TM3000 (Hitachi High-Tech Corp., Japan) and field emission scanning electron microscopes (FE-SEMs) SU8000 and S-4800 (Hitachi High-Tech Corp.). Bulk density was calculated from the volume and mass of samples cut into cubes. The relative error of the density determination, estimated from five independent measurements, was ≤3%. Porosity was calculated using the bulk density obtained from measurements and the true density values reported in the literature.[24]

Total reflectance in the ultraviolet–visible–near-infrared (UV–Vis–NIR) region was measured using a spectrophotometer V-770 (JASCO Corp.) equipped with an integrating sphere unit (ISN-923). A diffusive reflectance standard (Spectralon SRS-99-010, Labsphere, Inc.) was employed as the reference in all measurements. Mid-infrared (MIR) reflectance measurements were performed using a 10 cm gold-coated integrating sphere in conjunction with Fourier transform infrared spectrometer Nicolet iS20 (Thermo Fisher Scientific Inc.), with a gold diffuse reflector used as the reference.

Nitrogen gas adsorption and desorption measurements were carried out using BELSORP-max (MicrotracBEL Corp.). Before measurement, each sample was degassed under vacuum at 110°C for 12 h. The specific surface area was determined based on the Brunauer–Emmett–Teller (BET) method.

Thermogravimetry analysis (TGA) was performed using TG–DTA2000SR (Netzsch GmbH). The measurements were conducted under a flow of high-purity air at 150 mL min^{-1}, with a heating rate of 10°C min^{-1}. An aluminum pan served as the sample container, while α-alumina was used as the reference material. X-ray diffraction (XRD) measurements were conducted using MiniFlex600 (Rigaku Corp.) with Cu Kα radiation. Prior to measurement, the pre-dried samples were finely ground into a powder.

3 | RESULTS AND DISCUSSION

3.1 | Fabrication of hollow-structured monoliths

In this study, the method reported by Tokudome et al. was revisited with the aim of fabricating disk-shaped macroporous monoliths with a diameter of 25 mm (≈1 in).[19,20] While monoliths with diameters exceeding 10 mm could be formed using the same precursor composition as in previous studies, cracks developed during the drying process, making it difficult to obtain intact monoliths. Consequently, a modification was made to the composition of the reaction system, resulting in the fabrication of larger monoliths that were free of cracks. In this process, a stable sol–gel system was identified, consisting of aluminum chloride hexahydrate (5.0 g) as a precursor and PO as a proton scavenger in a 10 mL water–ethanol mixture (volume ratio 4:6).[25,26] The structural formation and characteristics of this system are discussed in detail below.

Figure 1 presents SEM images illustrating how the morphology of the samples varies with PEO content. In sol–gel-derived macroporous monoliths, the employment of phase separation inducers constitutes a well-established strategy for the control of macropore morphology. In line with this approach, PEO was added as a phase separation inducer in this study. As a first step, its effect was examined in a series of samples containing 4.0 mL of PO, designated as AM4-*y*. Composition-dependent morphological changes were observed as the PEO content increased from 0 to 0.08 g. This structural change reproduces what has been reported in previous studies,[19,20] and a composition AM4-0.04 exhibiting a bicontinuous structure was also confirmed. However, all samples in this system developed cracks when scaled above 10 mm, making them unsuitable for large monolith fabrication.

To address this size limitation, the PO content was increased to 6.0 mL (AM6-*y* system). Increasing the PO amount accelerated the pH rise and shortened the gelation time. These alterations resulted in the formation of wet gels that exhibited slightly diminished fragility. In these systems, crack-free monoliths with larger diameters were successfully fabricated, even after evaporative drying. While structural changes were observed upon the addition of PEO, these changes were less pronounced than those observed in the AM4-*y* system. The experimental process was successful in yielding crack-free monoliths with centimeter-scale diameters for all compositions. The diameter of the samples produced reached up to 50 mm without the incorporation of PEO (larger diameters were not explored).

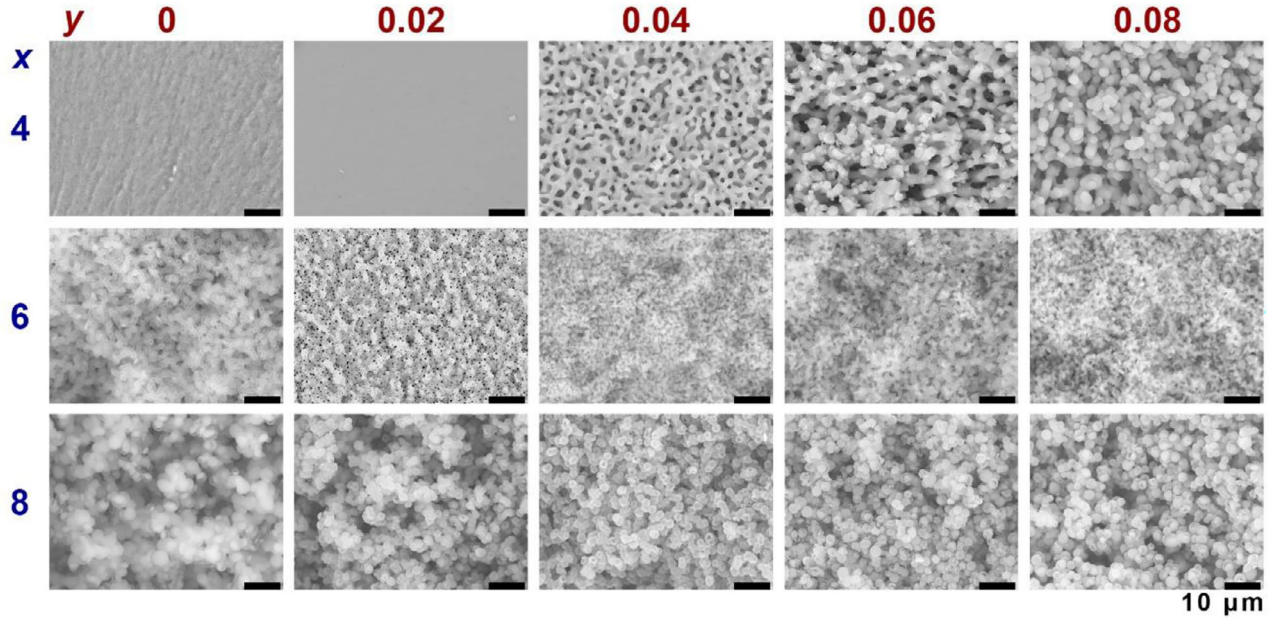

FIGURE 1 Scanning electron microscopy (SEM) images of aluminum hydroxide macroporous monoliths AM*x*-*y*.

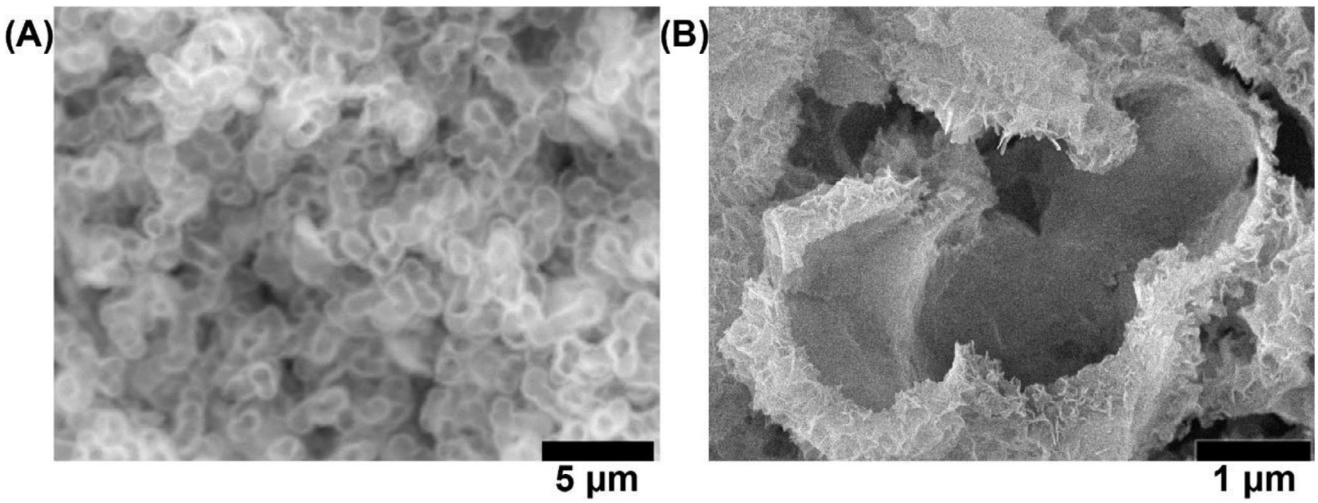

FIGURE 2 (A) Scanning electron microscopy (SEM) image of aluminum hydroxide monolith AM6-0. (B) Field emission scanning electron microscopy (FE-SEM) image of a fractured skeleton of AM6-0. A continuous hollow cavity network can be observed within the skeleton, and similar features were observed at multiple locations during imaging.

When the PO content was increased to 8.0 mL (AM8-*y* system), the system produced aggregates of spherical particles. The structural alterations resulting from the incorporation of PEO were minimal. When the PO exceeded 10 mL, gelation occurred within seconds after PO addition, which precluded sufficient stirring and prevented uniform monolith formation. In contrast, when the PO content was reduced below 3.0 mL, only white precipitates formed, and no monolithic gelation was observed.

A SEM analysis of the AM6-0 specimen revealed a continuous skeletal structure with highly contrasted regions on the surface (Figure 2). These regions, which exhibited a high degree of contrast, were initially presumed to be imaging artifacts. However, high-magnification FE-SEM observations (Figure 2B) confirmed that they corresponded to a structure consisting of aggregates of nanoplatelet-like domains with internal cavities. Although the XRD pattern (Figure 3B) shows broad features characteristic of an amorphous or poorly crystalline phase, the presence of nanoplatelet morphology suggests some degree of local order. To gain deeper insight into the crystallographic nature of these domains, advanced techniques such as high-resolution transmission electron microscopy

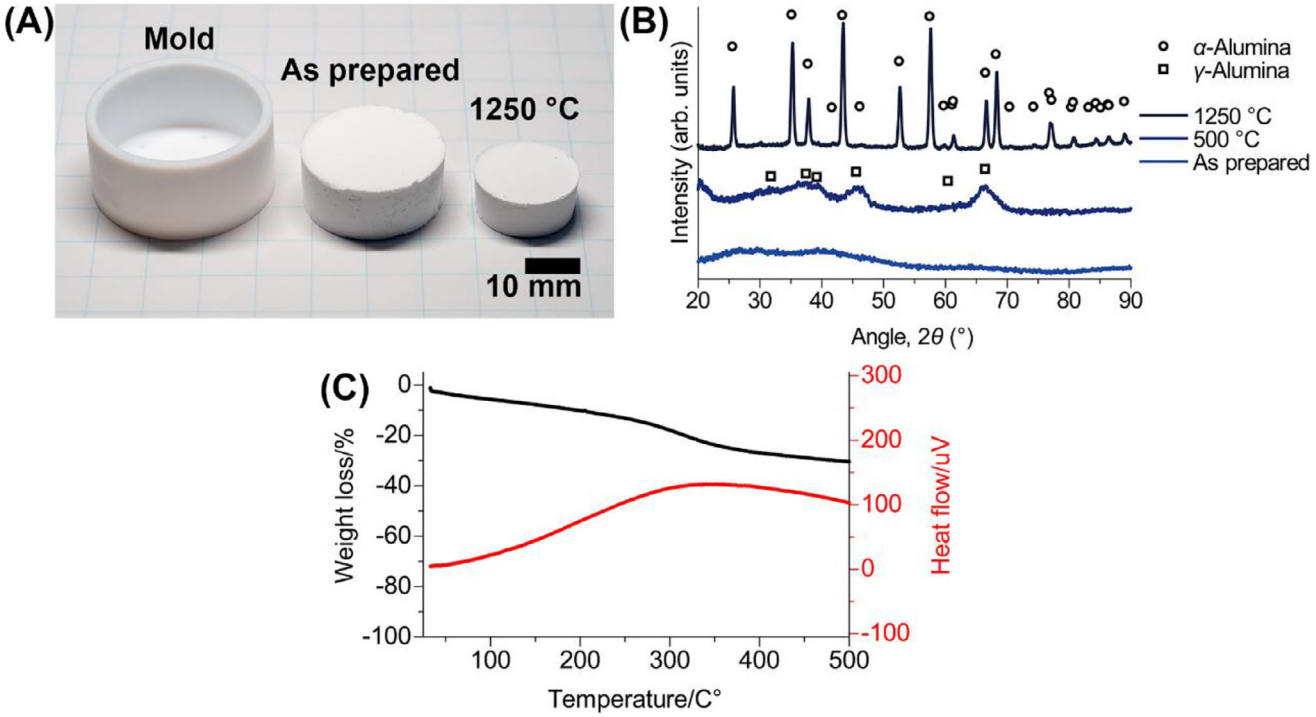

FIGURE 3 (A) Photograph of the mold used for gel preparation, the aluminum hydroxide monolith AM6-0, and the sample calcined at 1250°C. Although shrinkage occurs during aging, drying, and calcination, the monolithic shape is maintained. (B) X-ray diffraction (XRD) patterns of AM6-0 and its calcined samples. The material transitions from amorphous or nanocrystalline aluminum hydroxide to γ-alumina and eventually to α-alumina. (C) Thermogravimetric–differential thermal analysis (TG–DTA) curve of the as-prepared monolith (AM6-0) measured in air up to 500°C.

TABLE 1 Physical properties of aluminum hydroxide monolith AM6-0 and its calcined samples.

Calcination temperature	Bulk density (g cm^{-3})	Porosity (%)	BET specific surface area (m^2 g^{-1})
As prepared	0.152	93.8	429
500°C	0.174	95.2	314
1250°C	0.246	93.8	<10

Abbreviation: BET, Brunauer–Emmett–Teller.

or synchrotron-based analysis may be useful in future studies. The monolith manifested a chain-like morphology composed of interconnected spherical particles, forming a continuous hollow framework. Although AM8-0 also exhibited nanoplatelet shell structures, the hollow interiors were isolated and did not form a continuous network.

The AM6-0 monoliths were further calcined at temperatures up to 1250°C. Despite some shrinkage, the monolithic structure remained intact at all temperatures (Figure 3A). The bulk density increased with calcination, while the porosity did not decrease significantly, which is an important characteristic of this material (Table 1). TGA and XRD confirmed that the as-prepared material consisted of amorphous or nanocrystalline aluminum hydroxide. After heat treatment at 500°C, the sample exhibited a mass loss of approximately 35%, as determined by comparing the sample weights before and after heating, which is consistent with dehydration and the formation of γ-alumina. Although this transformation was supported by the XRD results, a distinct thermal event associated with dehydration was not clearly observed in the TGA curve (Figure 3B,C). The transformation into α-alumina at temperatures above 1200°C was confirmed by XRD, as the TGA measurement was limited to 500°C. These phase transitions caused shrinkage and microstructural changes due to dehydration and recrystallization of the nanoplatelet skeleton. At 500°C, the hollow morphology was preserved, and SEM images showed narrow necks between particles (Figure 4). At 1250°C, the outer walls of the hollow struc-

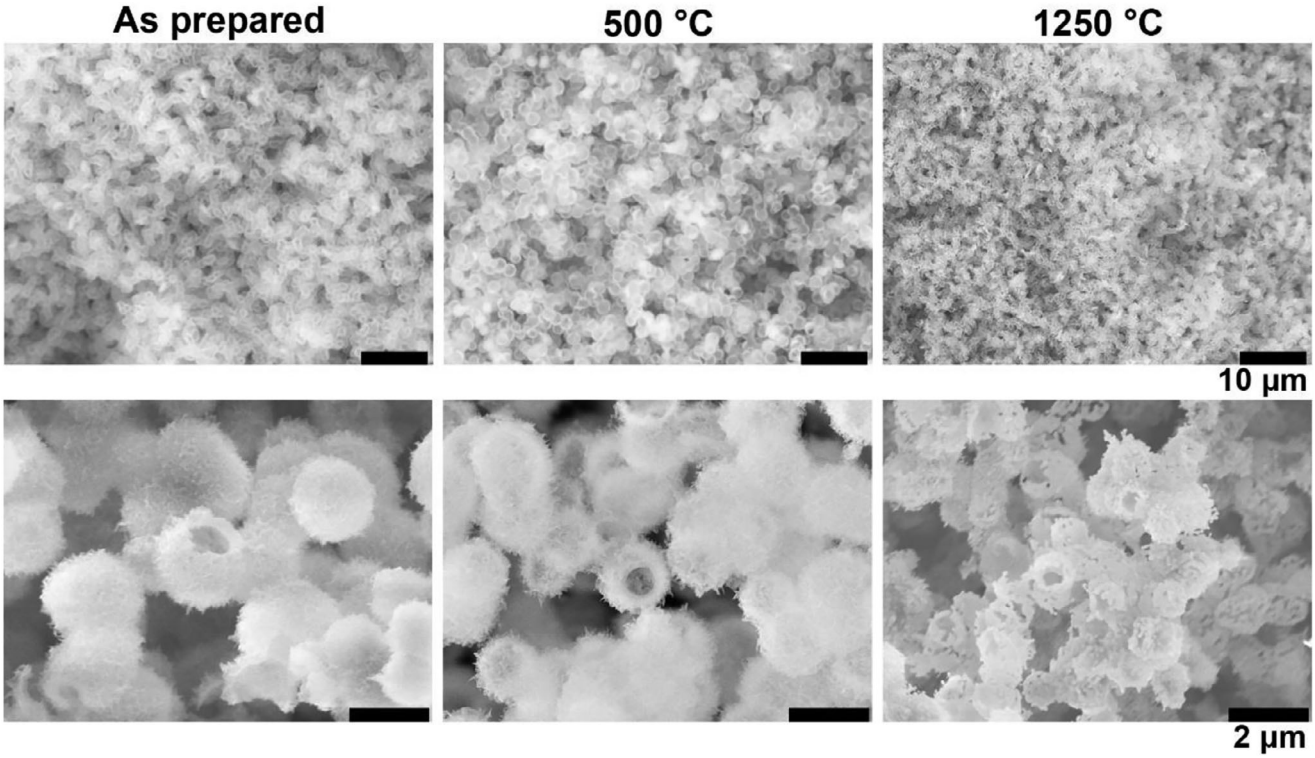

FIGURE 4 Field emission scanning electron microscopy (FE-SEM) images of AM6-0 and its calcined samples. The hollow structure is preserved after calcination at 500°C, whereas pores appear in the shell at 1250°C, resulting in the loss of the continuous hollow structure.

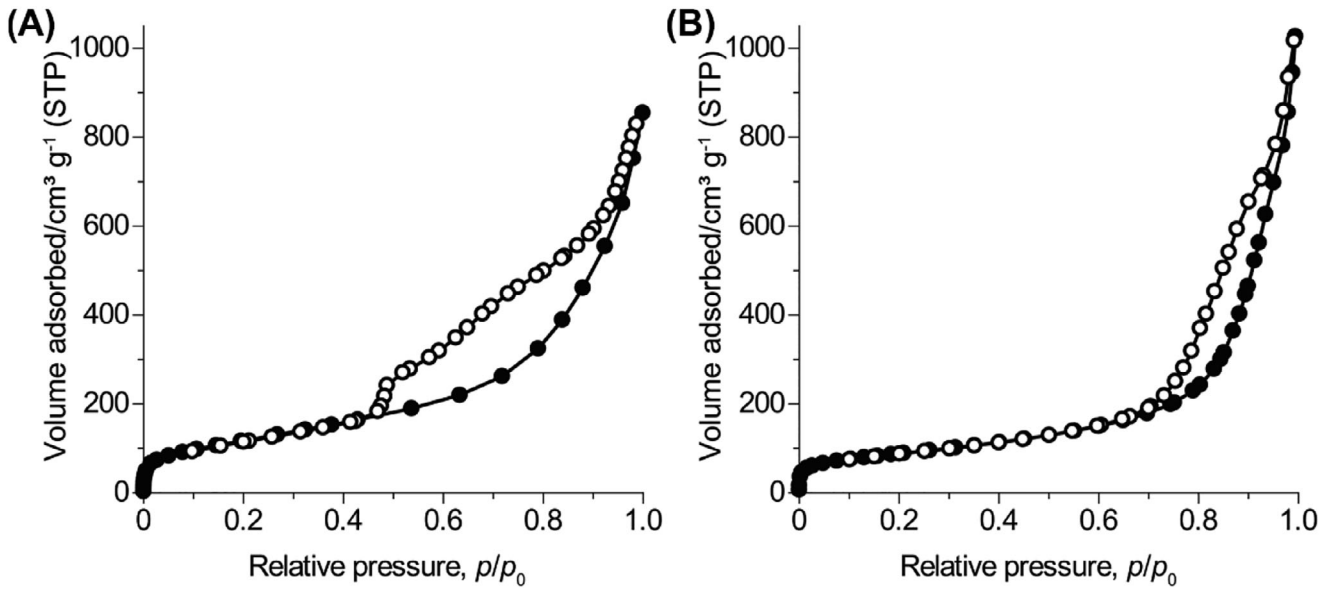

FIGURE 5 Nitrogen adsorption–desorption isotherms of (A) AM6-0 and (B) the sample calcined at 500°C. Reliable data could not be obtained for the 1250°C-calcined sample due to the collapse of pores and a significant decrease in surface area.

tures collapsed, resulting in discontinuity. Nevertheless, skeletal continuity was retained.

Nitrogen adsorption–desorption measurements revealed that both the as-prepared and the 500°C-calcined samples exhibited type IV isotherms with H3 hysteresis loops (Figure 5),[27,28] which is consistent with the nanoplatelet-based aluminum hydroxide structure observed in SEM. The BET specific surface areas were 429 and 314 $m^2\ g^{-1}$ for the as-prepared and 500°C-calcined samples, respectively. The decrease in specific surface

area and the narrowing of the hysteresis loop suggests that some mesopores collapsed during dehydration. In contrast, the 1250°C-calcined sample exhibited a significant reduction in surface area due to the formation of the α-phase, and reproducible isotherms could not be obtained. FE-SEM images confirmed structural densification, evidenced by a smooth skeleton surface devoid of mesopores; however, the monolithic form and overall continuity of the skeletal framework remained intact.

Although the formation mechanism of the hollow framework remains to be clarified, the following reaction pathway is proposed. In the presence of chloride ions, PO undergoes a ring-opening reaction that consumes protons and produces byproducts such as 1-chloro-2-propanol.[25,26] This raises the pH, inducing the precipitation of aluminum hydroxide.[19,20] These early byproducts are miscible with the ethanol–water solvent mixture. As the reaction proceeds, further condensation of these and related species is expected to yield more hydrophobic oligomers. The resulting decrease in solubility may induce phase separation, forming distinct domains within the gel. Aluminum hydroxide may preferentially precipitate at the interface of these domains, which could contribute to the formation of the hollow skeletal structure.[29] The formation of nanoplatelet aluminum hydroxide under pH 4–6 conditions has been reported previously,[30–34] which aligns with the reaction conditions used in this study. These processes likely lead to the formation of a three-phase structure consisting of a solvent phase, an aluminum hydroxide shell, and a PO-derived phase. This yields a hollow structure upon washing and drying. I also found that insufficient washing of AM6-0 before calcination at 500°C led to blackening of the sample. This blackening was attributed to thermal decomposition of residual PO-derived species within the aluminum hydroxide shell under oxygen-deficient conditions. To directly verify this hypothesis and extend it to other metal oxide systems, future studies will involve detailed structural and compositional analyses using synchrotron radiation and cryo-Raman microscopy in future work. This synthetic approach can be extended to other metal oxides (e.g., iron oxides)[26,35] and oxide–polymer hybrid composites.[36]

3.2 | Optical properties of the hollow-structured monoliths

Hollow particles are known to exhibit high light-scattering performance by inducing multiple scattering events through refractive index inhomogeneities created by internal voids.[22] When the particle size approaches the wavelength of visible light, Mie scattering becomes highly efficient.[37] Hollow particles composed of materials such as silica have been widely used as light-diffusing components, particularly in white coatings and reflective composites.[21–23,36] These systems take advantage of the internal voids and low absorption characteristics of silica (refractive index ~1.46 at 550 nm)[24] to achieve high reflectance across the visible spectrum. Alumina has a significantly higher refractive index (~1.76 at 550 nm for α-alumina) as well as superior thermal and chemical stability, making it an attractive candidate for broadband and high-temperature optical applications.[38] While dense alumina plates have been used as diffuse reflectors, systematic studies focusing on hollow-structured alumina particles or monoliths for light-scattering applications are scarce. To the best of my knowledge, porous alumina monoliths with internally hollow skeletal frameworks have not been investigated in detail for their broadband reflectance behavior, particularly in the MIR region. This study addresses that gap by evaluating the total diffuse reflectance of such alumina monoliths across the UV to MIR spectral regions.

Motivated by these considerations, I investigated the total diffuse reflectance of the as-prepared hollow aluminum hydroxide monoliths and their calcined counterparts to evaluate their potential use as light-diffusive reflective materials. Figure 6 shows the total reflectance spectra of the uncalcined aluminum hydroxide and the α-alumina monoliths calcined at 1250°C, measured across the near-UV, Vis, NIR, and MIR regions. Spectralon, a widely used standard for diffuse reflectance, was employed as the reference material. Both monoliths exhibited total diffuse reflectance equivalent to or higher than that of Spectralon in the wavelength range of 400–1200 nm. Spectralon is a widely used reflectance standard composed of sintered polytetrafluoroethylene. The material exhibits extremely low absorption and strong multiple scattering across a broad spectral range. High reflectance in the MIR region is attributed to the absence of strong vibrational absorption bands, unlike hydroxyl-containing or inorganic materials. Consistent with this, the aluminum hydroxide monolith showed slightly reduced reflectance in the NIR region due to absorption by surface hydroxyl groups. After calcination and transformation to the α-alumina phase, however, the material exhibited consistently high reflectance above 90%, showing clearly improved performance in the MIR region compared to the uncalcined sample.

These results suggest that the alumina monoliths developed in this study can be used as diffuse reflectance standards like Spectralon. These materials can be synthesized via a simple, low-cost, sol–gel-based process. Additionally, α-alumina maintains structural stability under extreme thermal conditions exceeding 2000°C. These materials

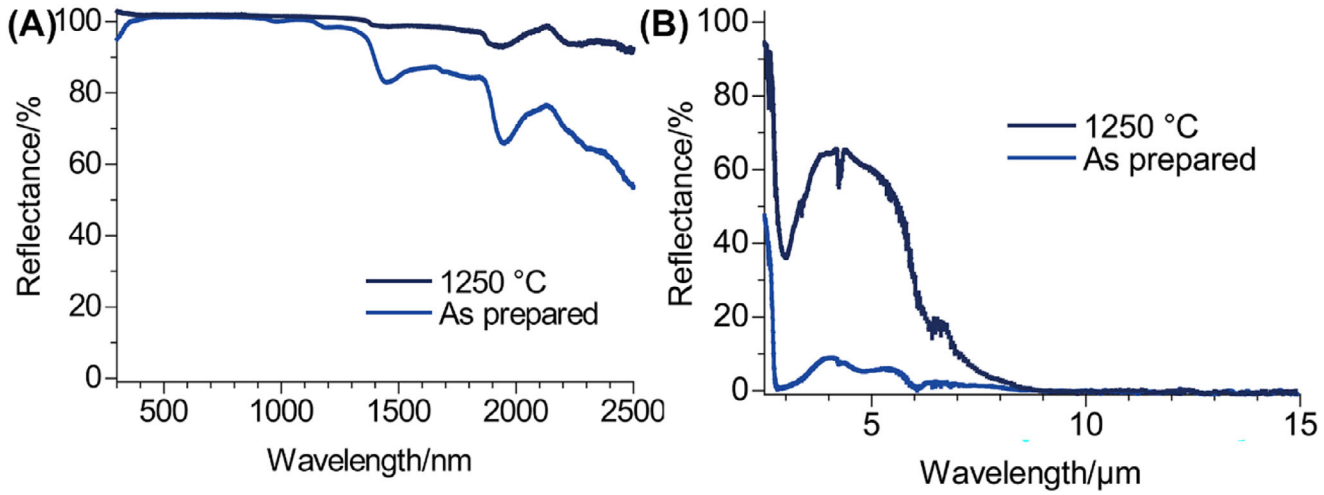

FIGURE 6 (A) Near-ultraviolet–visible–near-infrared (UV–Vis–NIR) and (B) mid-infrared (MIR) total reflectance spectra of the aluminum hydroxide monolith AM6-0 and its sample calcined at 1250°C.

could be used as durable white reflectance standards in high-temperature or infrared environments where Spectralon is not suitable. They could also be used in spectroscopic instruments or environmental sensing systems that require high-performance optical reference materials.

4 | CONCLUSION

Centimeter-scale macroporous aluminum hydroxide monoliths with continuous hollow skeletal frameworks were fabricated by combining metal–salt precursors with phase-separation-assisted sol–gel processing. The representative sample AM6-0 had a bulk density of 0.152 g cm^{-3}, corresponding to a porosity of 93.8%. The nanoplatelet-based shells formed a contiguous hollow network through bead-like junctions. The as-prepared sample exhibited a BET specific surface area of 429 m^2 g^{-1}. Calcination at 500°C dehydrated the framework into γ-alumina, preserving the architecture and yielding a specific surface area of 314 m^2 g^{-1}. Subsequent calcination at 1250°C produced α-alumina while preserving the monolithic form and the continuity of the skeletal framework; however, the hollow structure collapsed. The hollow monolith displayed total diffuse reflectance comparable to Spectralon over 400–1200 nm. The reflectance of the uncalcined material decreased in the MIR due to hydroxyl absorption. However, the α-alumina monolith retained over 90% diffuse reflectance in the NIR region up to 2500 nm.

The aluminum hydroxide monoliths and their calcined alumina derivatives can be synthesized via a simple, cost-effective process and offer a versatile platform for a range of applications. Potential uses include thermal insulation, white optical substrates, and durable reflectance standards for high-temperature spectroscopy. Their continuous hollow skeletons and interconnected pore networks enable functions such as adsorption, catalysis, and flow-through reaction media, comparable to those of conventional hierarchical porous materials. The fabrication of centimeter-scale monoliths with continuously hollow skeletons has not been previously reported. This approach may also be applicable to other compositionally similar oxide systems, offering a potential route to hollow monolithic materials with tunable structures.

ACKNOWLEDGMENTS

The author thanks Dr. Satoshi Ishii (National Institute for Materials Science) for helping with the MIR reflectance measurements. The author also acknowledges Dr. Yasuaki Tokudome (Osaka Metropolitan University) for kindly addressing questions regarding his previous publications. This work was supported by "Advanced Research Infrastructure for Materials and Nanotechnology in Japan" of the Ministry of Education, Culture, Sports, Science and Technology (MEXT) (proposal numbers JPMXP1223NM5285, JPMXP1224NM5101 and JPMXP1225NM5072).

CONFLICT OF INTEREST STATEMENT

The author declares no conflicts of interest.

ORCID

Gen Hayase https://orcid.org/0000-0003-1970-6129

REFERENCES

1. Feinle A, Elsaesser MS, Hüsing N. Sol–gel synthesis of monolithic materials with hierarchical porosity. Chem Soc Rev. 2016;45(12):3377–99. https://doi.org/10.1039/c5cs00710k

2. Triantafillidis C, Elsaesser MS, Hüsing N. Chemical phase separation strategies towards silica monoliths with hierarchical porosity. Chem Soc Rev. 2013;42(9):3833. https://doi.org/10.1039/C3CS35345A
3. Miyamoto R, Ando Y, Kurusu C, Bai H-Z, Nakanishi K, Ippommatsu M. Fabrication of large-sized silica monolith exceeding 1000 mL with high structural homogeneity. J Sep Sci. 2013;36(12):1890–96. https://doi.org/10.1002/jssc.201300123
4. Bao Y, Shi C, Wang T, Li X, Ma J. Recent progress in hollow silica: template synthesis, morphologies and applications. Microporous Mesoporous Mater. 2016;227:121–36. https://doi.org/10.1016/j.micromeso.2016.02.040
5. Wang Y, Tseng WJ. A novel technique for synthesizing nanoshell hollow alumina particles. J Am Ceram Soc. 2009;92(s1):S32–S37. https://doi.org/10.1111/j.1551-2916.2008.02653.x
6. Kato T, Ushijima H, Katsumata M, Hyodo T, Shimizu Y, Egashira M. Effect of core materials on the formation of hollow alumina microspheres by mechanofusion process. J Am Ceram Soc. 2004;87(1):60–67. https://doi.org/10.1111/j.1551-2916.2004.00060.x
7. Chatterjee M, Enkhtuvshin D, Siladitya B, Ganguli D. Hollow alumina microspheres from boehmite sols. J Mater Sci. 1998;33(20):4937–42. https://doi.org/10.1023/a:1004430218980
8. Wang F, Yuan X, Wang D. Hydrothermal synthesis of hierarchical boehmite (γ-AlOOH) hollow microspheres with highly active surface. AIP Adv. 2021;11(6):065209. https://doi.org/10.1063/5.0050294
9. Cai W, Yu J, Cheng B, Su B-L, Jaroniec M. Synthesis of boehmite hollow core/shell and hollow microspheres via sodium tartrate-mediated phase transformation and their enhanced adsorption performance in water treatment. J Phys Chem C. 2009;113(33):14739–46. https://doi.org/10.1021/jp904570z
10. Cai W, Yu J, Mann S. Template-free hydrothermal fabrication of hierarchically organized γ-AlOOH hollow microspheres. Microporous Mesoporous Mater. 2009;122(1–3):42–47. https://doi.org/10.1016/j.micromeso.2009.02.003
11. Cai W, Hu Y, Yu J, Wang W, Zhou J, Jaroniec M. Template-free synthesis of hierarchical γ-Al_2O_3 nanostructures and their adsorption affinity toward phenol and CO_2. RSC Adv. 2015;5(10):7066–73. https://doi.org/10.1039/c4ra11329b
12. Wu X, Wang D, Hu Z, Gu G. Synthesis of γ-AlOOH (γ-Al_2O_3) self-encapsulated and hollow architectures. Mater Chem Phys. 2008;109(2–3):560–64. https://doi.org/10.1016/j.matchemphys.2008.01.004
13. Pourmadadi M, Farokh A, Rahmani E, Shamsabadipour A, Eshaghi MM, Rahdar A, et al. Porous alumina as potential nanostructures for drug delivery applications, synthesis and characteristics. J Drug Deliv Sci Technol. 2022;77(103877):103877. https://doi.org/10.1016/j.jddst.2022.103877
14. Li B, Xiong J, Peng C, Li M, Liu H, Wang W, et al. Hierarchical porous AlOOH hollow microspheres for efficient CO_2 capture. Ceram Int. 2023;49(23):38226–36. https://doi.org/10.1016/j.ceramint.2023.09.154
15. Liu S, Shah M, Rao S, Mohammadi MM, Kumar A, Ren S, et al. Flame aerosol synthesis of hollow alumina nanoshells for application in thermal insulation. Chem Eng J. 2022;428(131273):131273. https://doi.org/10.1016/j.cej.2021.131273
16. Dong H, Xie R, Yang L, Li F. A hierarchical flower-like hollow alumina supported bimetallic AuPd nanoparticle catalyst for enhanced solvent-free ethylbenzene oxidation. Dalton Trans. 2018;47(23):7776–86. https://doi.org/10.1039/c8dt01182f
17. Korhonen JT, Hiekkataipale P, Malm J, Karppinen M, Ikkala O, Ras RHA. Inorganic hollow nanotube aerogels by atomic layer deposition onto native nanocellulose templates. ACS Nano. 2011;5(3):1967–74. https://doi.org/10.1021/nn200108s
18. Biener MM, Ye J, Baumann TF, Wang YM, Shin SJ, Biener J, et al. Ultra-strong and low-density nanotubular bulk materials with tunable feature sizes. Adv Mater. 2014;26(28):4808–13. https://doi.org/10.1002/adma.201400249
19. Tokudome Y, Fujita K, Nakanishi K, Miura K, Hirao K. Synthesis of monolithic Al_2O_3 with well-defined macropores and mesostructured skeletons via the sol−gel process accompanied by phase separation. Chem Mater. 2007;19(14):3393–98. https://doi.org/10.1021/cm063051p
20. Tokudome Y, Nakanishi K, Kanamori K, Fujita K, Akamatsu H, Hanada T. Structural characterization of hierarchically porous alumina aerogel and xerogel monoliths. J Colloid Interface Sci. 2009;338(2):506–13. https://doi.org/10.1016/j.jcis.2009.06.042
21. Xing Z, Tay S-W, Ng YH, Hong L. Porous SiO_2 hollow spheres as a solar reflective pigment for coatings. ACS Appl Mater Interfaces. 2017;9(17):15103–13. https://doi.org/10.1021/acsami.6b16760
22. Fujiwara M, Shiokawa K, Sakakura I, Nakahara Y. Preparation of hierarchical architectures of silica particles with hollow structure and nanoparticle shells: a material for the high reflectivity of UV and visible light. Langmuir. 2010;26(9):6561–67. https://doi.org/10.1021/la9043396
23. Kim J, Lee C, Suh YJ, Chang H, Roh K-M, Jang HD. Synthesis and characterization of highly reflective hollow silica particles. Mater Res Bull. 2015;70:184–89. https://doi.org/10.1016/j.materresbull.2015.04.046
24. Shackelford JF, Doremus RH. Ceramic and glass materials: structure, properties and processing. New York, NY: Springer; 2008. https://doi.org/10.1007/978-0-387-73362-3
25. Gash AE, Satcher JH, Simpson RL. Strong Akaganeite aerogel monoliths using epoxides: synthesis and characterization. Chem Mater. 2003;15(17):3268–75. https://doi.org/10.1021/cm034211p
26. Gash AE, Tillotson TM, Satcher JH, Poco JF, Hrubesh LW, Simpson RL. Use of epoxides in the sol−gel synthesis of porous iron(III) oxide monoliths from Fe(III) salts. Chem Mater. 2001;13(3):999–1007. https://doi.org/10.1021/cm0007611
27. Thommes M, Kaneko K, Neimark AV, Olivier JP, Rodriguez-Reinoso F, Rouquerol J, et al. Physisorption of gases, with special reference to the evaluation of surface area and pore size distribution (IUPAC Technical Report). Pure Appl Chem. 2015;87(9–10):1051–69. https://doi.org/10.1515/pac-2014-1117
28. Sing K. The use of nitrogen adsorption for the characterisation of porous materials. Colloids Surf A. 2001;187–188:3–9. https://doi.org/10.1016/S0927-7757(01)00612-4
29. Herzberger J, Niederer K, Pohlit H, Seiwert J, Worm M, Wurm FR, et al. Polymerization of ethylene oxide, propylene oxide, and other alkylene oxides: synthesis, novel polymer architectures, and bioconjugation. Chem Rev. 2016;116(4):2170–243. https://doi.org/10.1021/acs.chemrev.5b00441
30. Zhang X, Cui W, Hu JZ, Wang H-W, Prange MP, Wan C, et al. Transformation of gibbsite to boehmite in caustic aque-

ous solution at hydrothermal conditions. Cryst Growth Des. 2019;19(10):5557–67. https://doi.org/10.1021/acs.cgd.9b00468
31. Zhang H, Zhang X, Graham TR, Pearce CI, Hlushko H, LaVerne JA, et al. Crystallization and phase transformations of aluminum (oxy)hydroxide polymorphs in caustic aqueous solution. Inorg Chem. 2021;60(13):9820–32. https://doi.org/10.1021/acs.inorgchem.1c01111
32. Wang S, Zhang X, Graham TR, Zhang H, Pearce CI, Wang Z, et al. Two-step route to size and shape controlled gibbsite nanoplates and the crystal growth mechanism. CrystEngComm. 2020;22(15):2555–65. https://doi.org/10.1039/d0ce00114g
33. Zhang X, Zhang X, Graham TR, Pearce CI, Mehdi BL, N'Diaye AT, et al. Fast synthesis of gibbsite nanoplates and process optimization using box-Behnken experimental design. Cryst Growth Des. 2017;17(12):6801–8. https://doi.org/10.1021/acs.cgd.7b01400
34. Zhang X, Huestis PL, Pearce CI, Hu JZ, Page K, Anovitz AB, et al. Boehmite and gibbsite nanoplates for the synthesis of advanced alumina products. ACS Appl Nano Mater. 2018;1(12):7115–28. https://doi.org/10.1021/acsanm.8b01969
35. Ma F-X, Hu H, Wu HB, Xu CY, Xu Z, Zhen L, et al. Formation of uniform Fe_3O_4 hollow spheres organized by ultrathin nanosheets and their excellent lithium storage properties. Adv Mater. 2015;27(27):4097–101. https://doi.org/10.1002/adma.201501130
36. Ernawati L, Ogi T, Balgis R, Okuyama K, Stucki M, Hess SC, et al. Hollow silica as an optically transparent and thermally insulating polymer additive. Langmuir. 2016;32(1):338–45. https://doi.org/10.1021/acs.langmuir.5b04063
37. van de Hulst HC. Light scattering by small particles. Mineola, NY: Dover Publications; 1981
38. Li R, Kodaira T, Kawanami H. In situ formic acid dehydrogenation observation using a UV-vis-diffuse-reflectance spectroscopy system. Chem Commun. 2022;58(79):11079–82. https://doi.org/10.1039/d2cc03768h

How to cite this article: Hayase G. Hollow skeletal macroporous aluminum hydroxide monoliths and their calcined derivatives with high diffuse reflectance. J Am Ceram Soc. 2026;109:e70276. https://doi.org/10.1111/jace.70276